Environmental Science Processes & Impacts

ROYAL SOCIETY OF CHEMISTRY

PAPER

View Article Online
View Journal

Cite this: DOI: 10.1039/d6em00129g

Carbon and nutrient mobilization across inundation gradients in an emerging freshwater delta

Matthew J. Berens, † Geoff Schwaner and Elizabeth M. Herndon *

Emerging freshwater deltas are comprised of gradients of soil age and inundation frequency that influence biogeochemical processes. Differences in inundation patterns coupled with soil chemical properties may affect whether carbon and nutrients transported from inland watersheds are stored in delta soils or released into the atmosphere or open ocean. This study uses laboratory incubations to evaluate the responses of soil, porewater, and headspace parameters to different inundation patterns in soils collected from two elevation transects of an emerging deltaic island in the Wax Lake Delta in Louisiana, USA, an active freshwater delta forming along the Louisiana coast in response to water diversions. In general, soils from the older region of the island exhibited higher CO_2 release and solute mobilization relative to soils from the younger delta region. In addition, persistent inundation was associated with significantly lower solute (DOC, Fe, P) and CO_2 release than soil exposed to persistently drained conditions or periodic flood–drain cycles. Our results indicate that biogeochemical processes, such as organic matter decomposition and microbial Fe cycling, may be limited by inundated conditions in subtidal zones but vary in response to differences in soil chemical properties (*e.g.*, C and N content) across supratidal and intertidal regimes. These results demonstrate that hydrogeomorphic development, in addition to inundation patterns, regulate biogeochemical processes that produce solutes and gases in coastal systems.

Received 18th February 2026
Accepted 29th April 2026

DOI: 10.1039/d6em00129g

rsc.li/espi

Environmental significance

Emerging freshwater deltas influence the fate of C and nutrients exported from inland waters, with elevation and inundation gradients shaping soil biogeochemical processes. This study clarifies how soil chemical properties and inundation regulate C and P release from emerging deltaic systems. Older soils support greater biogeochemical activity in supratidal and intertidal zones, likely reflecting higher soil C concentrations. Inundation-driven redox oscillations in intertidal zones enhance OM decomposition to CO_2 and accelerate Fe(III) (oxyhydr)oxide turnover, whereas persistent subtidal saturation restricts O_2 availability and inhibits Fe–OC and Fe–P associations, though microbial Fe reduction may sustain OM decomposition and P release under anoxic conditions. This study advances understanding of how hydrogeomorphic development and Fe redox cycling jointly govern C storage and nutrient buffering in active coastal deltas.

Introduction

Coastal zones contain hydrologically dynamic ecosystems that receive freshwater from inland watersheds before it is discharged to the ocean. Within coastal ecosystems, interactions between land, freshwater, and seawater influence the cycling of solutes and particulates, and support key ecosystem services including carbon storage, nutrient buffering, and mitigation of flooding and storm surges.[1,2] In many coastal systems, sea level rise and alterations to rivers and streams (*e.g.*, river impoundment, groundwater extraction, land-use conversion) are causing extensive inundation and land erosion.[3–5] River diversions are a proposed approach to offset these losses by directing freshwater and sediment flows towards degrading coastlines to accelerate the vertical accretion of new land.[6–8] These diversions may alter the biogeochemical conditions of coastal zones by increasing the supply of carbon, nutrients (*i.e.*, N and P), and iron (Fe) while simultaneously lowering salinity.[9] An improved understanding of soil biogeochemistry in coastal ecosystems that are gaining land due to river diversions is critical for determining the impact of these activities on future carbon and nutrient cycling.

Deltas that form in response to river diversions are characterized by freshwater-dominated channels and a series of aggrading islands that span gradients of time since subaerial emergence and frequency of inundation.[10,11] Soils at the proximal (upstream) end and along the natural embankments around the perimeter of the islands are often older, reach higher elevations, and have higher organic matter content

Environmental Sciences Division, Oak Ridge National Laboratory, Oak Ridge, TN 37830, USA. E-mail: herndonem@ornl.gov

† Current address: Department of Environmental Engineering and Earth Sciences, Clemson University, Clemson, SC 29643, USA.

relative to distal (downstream) sedimentation regions and the interdistributary bays that comprise the island interiors.[12] The resulting elevation gradients spanning both upstream to downstream and from exterior to interior of the growing islands yield distinct hydrogeomorphic zones defined by ground surface elevation relative to the tidal range: supratidal (primarily drained at the ground surface); intertidal (periodically inundated by tides); or subtidal (consistently inundated). These zones contain characteristic vegetation ranging from emergent aquatic plants in subtidal areas (*e.g.*, *Nelumbo lutea*, *Lemma minor*) to wetland forest and herbaceous wetland species at higher elevations (*e.g.*, *Salix nigra*, *Colocasia esculenta*, *Polygonum punctatum*).[11,13,14] While several studies have described the sedimentation and vegetation patterns of emerging deltas, fewer studies have examined the effects of variable inundation on soil and porewater chemistry across elevation gradients.[15–17]

Carbon and nutrient dynamics in coastal systems are strongly influenced by redox-driven biogeochemical processes. In particular, variable inundation due to (semi-)diurnal tidal cycles and/or periods of low or elevated river discharge can oscillate soils between oxic and anoxic conditions, potentially resulting in the formation and/or dissolution of reactive Fe minerals (*i.e.*, Fe(III) oxides and oxyhydroxides).[18,19] When oxygen is depleted under flooded conditions, short range ordered (SRO) Fe(III) oxyhydroxides (*e.g.*, ferrihydrite) may act as terminal electron acceptors for microbial respiration, promoting the decomposition of organic carbon into greenhouses gases (*i.e.*, carbon dioxide (CO_2)).[20] In addition, Fe(III) oxyhydroxides may strongly adsorb organic matter, nutrients, and trace elements which can then be released into soil porewaters *via* reductive mineral dissolution.[21] As soil moisture decreases with receding tides and/or river stage, soil pore spaces become aerated, causing the oxidative precipitation of dissolved or complexed Fe(II) into new solid Fe(III) phases. This formation of iron minerals could potentially stabilize large amounts of carbon and nutrients through adsorption and/or coprecipitation and increase carbon retention in deltaic soils.[17,18,22–28] While Fe redox cycling is recognized as a key process in coastal wetlands, its relative importance compared to other factors (*e.g.*, soil age and composition) in controlling C and nutrient dynamics across inundation gradients in freshwater deltas remains unclear.

The objectives of this study were to (i) investigate how CO_2 production and solute mobility respond to different inundation conditions across an emerging freshwater delta and (ii) to assess how Fe mineral precipitation and dissolution may affect solute immobilization and release. Surface soils (<30 cm) collected from supratidal, intertidal, and subtidal zones along two elevation transects in the Wax Lake Delta representing different timepoints of island development were incubated in laboratory mesocosms under conditions that reflected those experienced in the field: static drained (supratidal); repeated flood–drain cycles (intertidal); or static inundated (subtidal).[10,11] Mesocosms were assessed for differences in greenhouse gas emissions (CO_2, CH_4, N_2O) and the release of redox-sensitive analytes (DOC, Fe), nutrients (P), and cations (Ca, Mg, Al) into soil porewater. The concentrations of soil Fe contained in SRO and long range ordered (LRO) Fe(III) (oxyhydr)oxide minerals were quantified before and after incubation using selective chemical extractions.

Methods

Site description

The Wax Lake Delta (WLD) is located approximately 30 km southwest of Morgan City in Coastal Louisiana, USA (Fig. 1). This region experiences an annual precipitation of 1530 mm per year and daily mean temperatures ranging from 12 to 29 °C in winter and summer, respectively.[29] Wax Lake Delta is an active delta forming from sediments delivered through the Wax Lake Outlet, a channel constructed in 1941 to reduce flood stages in Coastal Louisiana communities by diverting a portion of the flow from the Atchafalaya River.[30] The resulting high sediment load (25.6–38.4 Mt yr^{-1})[31] in the Wax Lake Outlet has created a series of rapidly aggrading islands that initially became subaerial following a major flood in 1973 and now consist of a range of freshwater habitats (mean channel salinity 0.11 ± 0.004 ppt)[32] spanning forested wetlands to herbaceous marshes.

Wax Lake Delta exhibits distinct hydrogeomorphic zones defined by soil elevation, water level, and frequency of inundation.[10,11,33] Supratidal zones of the WLD are above the mean high water level (>0.3 m NAVD88) and inundated only during seasonal and extreme high-water events. These areas occur along the natural levees that border the islands and contain early successional woody vegetation, including black willow (*Salix nigra*) and elephant ear (*Colocasia esculenta*). Intertidal zones are between mean high and low water level (−0.4 to 0.3 m NAVD88) and experience regular flood–drain cycles, while subtidal zones (<−0.4 m NAVD88) are persistently inundated year-round. The water level in these zones is primarily influenced by river stage, wind, and storms and partly driven by (semi-)diurnal tides (<0.3 m total water level change).[12,34] Emergent forbs (*e.g.*, *Sagittaria* spp) and American lotus (*Nelumbo lutea*) are common in periodically-inundated intertidal zones, while emergent macrophytes dominate the subtidal zones (*e.g.*, *Eichhornia* spp., *Nymphaea* spp.).

Soils in the WLD also display clear vertical and lateral differentiation across hydrogeomorphic zones.[17,35,36] The sediment being transported to and deposited within the WLD is dominated by coarse silt to very fine sand materials.[37,38] Frequent inundation and sediment resuspension in subtidal zones maintains mineral-rich, fine-grained soils with high water content, low bulk density (mean 0.24 g cm^{-3}), and minimal organic carbon (<0.02 g cm^{-3}). Intertidal zones that experience periodic inundation support dense vegetation that traps sediment and contributes organic matter, resulting in more consolidated soils (mean bulk density 0.68 g cm^{-3}), with slightly elevated organic carbon (~0.01 g cm^{-3}) and shallow redox gradients. In supratidal zones, soils are infrequently flooded, more oxidized, and increasingly organic-rich (~0.02 g cm^{-3}), showing early pedogenic features and greater root biomass.

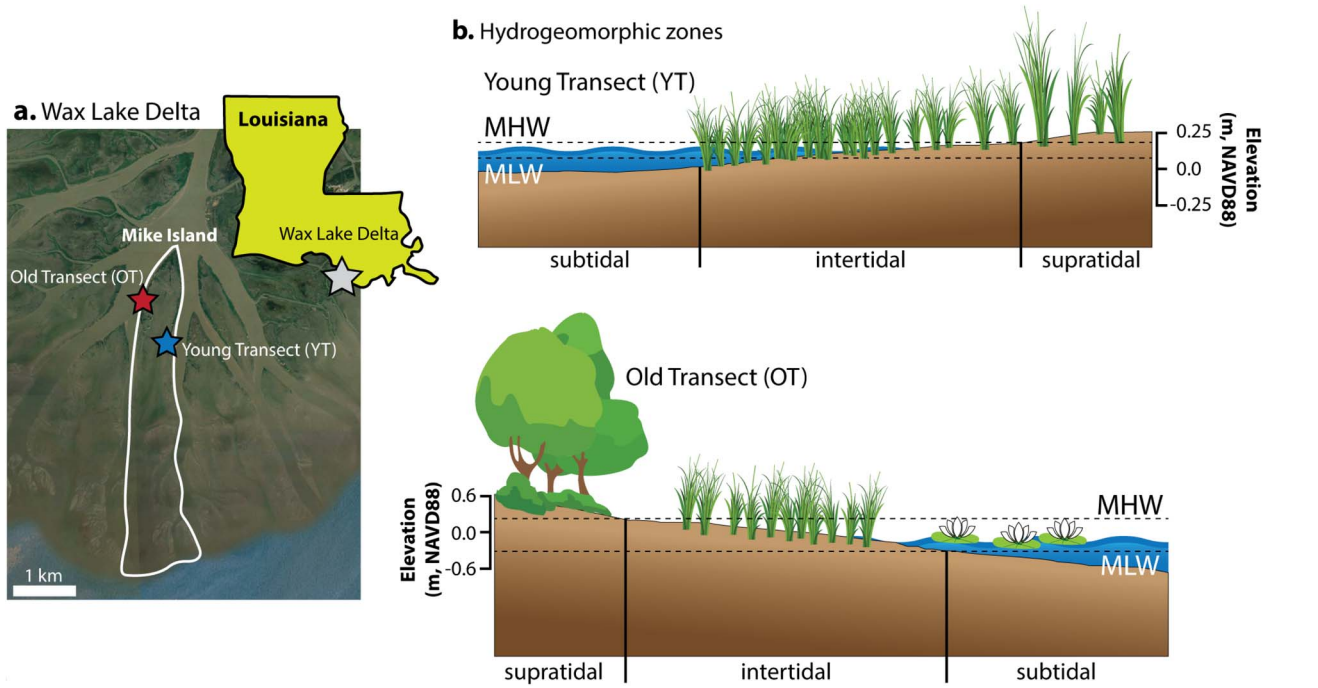

Fig. 1 (a) Map of Old Transect (OT) and Young Transect (YT) study sites on Mike Island in the Wax Lake Delta, Louisiana. (b) Conceptual illustration of hydrogeomorphic zones at Old Transect (OT) and Young Transect (YT) study areas. Approximate ground surface elevations and ecological zones are derived from Twilley *et al.* (2019).[10]

Soil collection

Surface soils were collected from two elevation transects on Mike Island in the WLD that exhibit differences in time since subaerial emergence, soil properties, and vegetation types (Fig. 1b). The "Old Transect" (OT; 29.51009, −91.44449) is in the proximal sedimentation region of Mike Island and first became subaerial between 1987–1995, whereas the "Young Transect" (YT; 29.49438, −91.44121) is closer to the active delta front and became subaerial between 2001–2005 (Fig. S1).[11] The OT exhibits pronounced ecological succession along the island's elevation gradient, transitioning from forested wetlands (primarily *Salix nigra*) in supratidal zones to marsh dominated species in intertidal (*e.g.*, *Sagittaria* spp., *Colocasia* spp.) and subtidal regions.[39–41] The YT includes primarily intertidal and subtidal hydrogeomorphology with vegetation mainly consisting of sawgrass and submerged and floating-leafed (*Potamogeton nodosus*) vegetation.[42,43] In the text, we use "Old Transect" and "Young Transect" strictly to reference the island age (*i.e.*, time since subaerial emergence) rather than features of soil development and/or weathering.

Triplicate shallow soil cores (0–30 cm depth) were collected in March 2023 from within a 1 m × 1 m plot at each sampling location by manually inserting a 5 cm diameter acrylic soil core liner (AMS, Inc.) into the soil until the 30 cm core liner was flush with the ground surface. The core liners were immediately capped and sealed in gas impermeable bags containing an oxygen-scrubbing pouch (AnaeroPack™, Mitsubishi Chemical Corp.) to preserve anoxic conditions. Soils experienced compaction during sampling that resulted in each core liner containing headspace derived from the subsurface environment. The samples were held on ice and frozen within 6 h of collection, then shipped overnight to Oak Ridge National Laboratory and stored at −20 °C until further processing.

Mesocosm setup and initial soil characterization

Incubation mesocosms were constructed from the acrylic core liners used for soil collection (diameter 5 cm, height 30 cm;

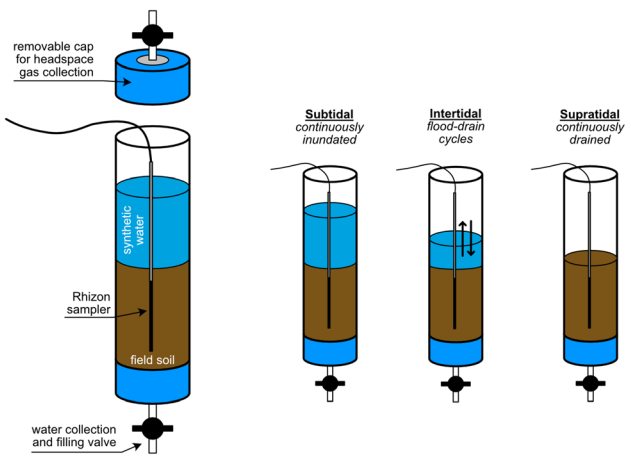

Fig. 2 Schematic of mesocosms used for laboratory soil incubations. (left) Example mesocosm containing field-collected soil and synthetic water. The valve at the bottom was used to fill and drain the mesocosms while the Rhizon sampler was used to collect *in situ* porewater. The removable cap was periodically attached to the top of each mesocosm for headspace gas collection. (right) Illustration of the three different incubation conditions. All mesocosms were constructed identically regardless of reaction conditions.

Fig. 2). The frozen soils were placed in an anaerobic chamber (97.5% N_2: 2.5% H_2; Coy, Inc.) and allowed to thaw completely at room temperature (~12 h). The thawed soils were removed from the liners, transferred into a 1 L acid-washed glass crystallization dish, and manually homogenized with an acid-washed glass rod and subsampled for pH (1 : 1 in 0.01 M $CaCl_2$), total C and N (Elementar UNICUBE®), and selective chemical extractions. After subsampling soils for initial characterization, they were then transferred back into the core liners, and the bottom cap was replaced with a cap containing a two-way valve to allow controlled drainage of the mesocosm. A layer of polyester filter cloth (5 μm pore size) was placed inside the cap to prevent the loss of soil while draining and filling the mesocosms. Due to limited quantities of soil from the OT intertidal zone, the triplicate soil samples were combined, homogenized, and split into duplicate mesocosms; all other incubations were performed in triplicate.

Selective chemical extractions were performed inside the anaerobic chamber to quantify concentrations of Fe and P associated with different solid Fe mineral phases. Subsamples for the extractions were dried under N_2 atmosphere in the glove box. The iron extractions followed previously described methods.[27,44,45] Briefly, short-range ordered (SRO) Fe(III) oxyhydroxides (*e.g.*, ferrihydrite, lepidocrocite) were extracted for 48 h with 1 M hydroxylamine-HCl in 25% (v/v) acetic acid. Total redox-sensitive Fe(III) (oxyhydr)oxides were extracted for 2 h with freshly prepared citrate-buffered sodium dithionite (50 g L^{-1} sodium dithionite in 0.35 M acetic acid and 0.2 M sodium citrate buffer, pH 4.8). Long-range ordered (LRO) Fe(III) oxide minerals (*e.g.*, crystalline goethite, hematite) were calculated as the difference between total-redox sensitive Fe(III) (oxyhydr)oxides and SRO Fe(III) oxyhydroxides. Each extraction protocol was performed by placing ~1.0 g of dried soil and 10 mL of the extractant solution in a 50 mL conical tube on an end-over-end rotator. The resulting soil slurries were centrifuged (30 min at 4000 rcf), and the supernatants were filtered (<0.45 μm nylon syringe filter) and acidified with 2–3 drops of trace metal grade nitric acid for analysis by inductively coupled plasma-optical emission spectroscopy (ICP-OES; ThermoFisher Scientific iCAP 7400).

Mesocosm incubation and sampling

The constructed mesocosms were transferred to the benchtop and incubated for 30 days at room temperature (20–22 °C) to match the mean annual temperature of the Wax Lake Delta (20.3 °C). To reflect field inundation conditions, supratidal mesocosms were incubated without additional water for 21 days, at which point the soils were rewetted to approximately field capacity due to visible drying of the soils. Because soil moisture was not measured in the field, field capacity was visually estimated by adding water until soils appeared moist throughout but not saturated. Subtidal mesocosms were continuously inundated at 15 cm above the soil surface to reflect the average water depth of the subtidal zone on Mike Island.[34] Intertidal mesocosms underwent four flood–drain cycles over the 30-day experiment. The composition of the solution used to inundate the intertidal soils reflected the concentrations of major ions measured in surface water at the field site during soil collection (100 μmol L^{-1} sulfate from Na_2SO_4, 420 μmol L^{-1} chloride from NaCl; see additional details in Table S1). The solution was prepared in deionized water and did not contain any solutes other than sodium, chloride, and sulfate. The first porewater measurement during the incubations captured the initial concentrations of solutes derived from the soil. The solution pH was 7.5, as prepared, and was not adjusted before use. During the flood–drain cycles, water from the intertidal mesocosms was gravity drained from the port on the bottom end cap. After the water was allowed to self-drain, any water that remained pooled on the soil surface was carefully removed by using a syringe connected to the port on the bottom cap to apply vacuum. For subsequent inundated periods, the water level was returned to 15 cm above the soil surface by slowly injecting fresh synthetic water upwards through the port on the bottom of the mesocosms, taking care to avoid disturbing the soil.

Before beginning the incubations, one Rhizon porewater sampler (0.15 μm pore size, 10 cm membrane length; Rhizosphere Research Products) was installed vertically into the center of the soil and left in place throughout the duration of the experiment. The rhizon spanned the top 10 cm of the mesocosm soil. The top of each mesocosm was loosely covered with semi-transparent plastic film to prevent evaporation and drying. Porewater from subtidal and intertidal mesocosms was collected through an acid-washed syringe (10% HCl) attached to the Rhizon sampler and subsequently analyzed for concentrations of dissolved organic C (DOC), P, Ca, Mg, total Fe, and Fe^{2+}, pH, specific conductance, and oxidation–reduction potential (ORP; mV *vs.* Ag/AgCl). Porewater was not collected from supratidal mesocosms due to insufficient volume available for chemical analyses. Dissolved organic carbon was measured with a total organic carbon analyzer (Shimadzu TOC-L). Total dissolved elements were quantified by ICP-OES. Concentrations of Fe^{2+} were quantified by the 1,10-phenanthroline assay in a UV-vis spectrophotometer.[46] Specific conductance, pH, and ORP were measured with a handheld multiparameter probe. ORP values were converted (+209 mV) to redox potentials relative to the standard hydrogen electrode (E_h).

To maintain a consistent water volume in each mesocosm, the volume of water removed during each sampling (~20 mL) was immediately replaced with fresh solution. At the end of the experiment, the mesocosms were transferred back into the anerobic chamber, the soils were removed from the liners and homogenized, then analyzed for total C and N concentrations and hydroxylamine and dithionite-extractable Fe and P.

Carbon dioxide flux measurements

Carbon dioxide (CO_2) fluxes (as mmol CO_2–C m^{-2} d^{-1}) were determined by sealing the mesocosms with a cap fitted with a butyl rubber septum (Fig. 2) and collecting a 15 mL aliquot of headspace gas three times over a 24 h period. The CO_2 concentrations were measured by gas chromatography (GC; Shimadzu Corp.). Flux values were calculated according to eqn (1):

$$\text{Soil } CO_2 \text{ flux} = \frac{\partial c}{\partial t} \times \frac{V}{A_S} \quad (1)$$

where c is the concentration of CO_2 in the headspace (in ppm_v), V is the headspace volume of each mesocosm (in m^3), A_s is the soil surface area (19.6 cm^2), and t is the total collection time (in hr). A linear regression of the three concentration measurements made during each 24 h collection period ($\partial c/\partial t$) was applied to determine the CO_2 flux. To account for the differences in soil C concentration across sites, CO_2 fluxes were normalized to the total C concentration in the initial bulk soils (in mol CO_2–C mol C^{-1}). Methane (CH_4) and nitrous oxide (N_2O) were also measured and were below the detection limit in all samples.

Data and statistical analysis

All data analyses were performed using in R (v4.3.0).[47] We used *dplyr* (v1.1.4) for data wrangling and processing; *ggplot2* (v3.5.2)[48] and *cowplot* (v1.2.0) for data visualization; and stats (v4.5.2) and *vegan* (v2.7–2) for multivariate statistics. We used PERMANOVA (Bray–Curtis; permutations: 999) to evaluate overall trends across transect location (OT *vs.* YT) and transect position (supratidal *vs.* intertidal *vs.* subtidal). Linear mixed-effects models (LME) and ANOVA were used to determine trends of individual analytes and compare means. Statistical significance was determined at $\alpha = 0.05$. Values of F and p reported in the text are from PERMANOVA analyses, unless otherwise stated. All analytical results with uncertainties are reported as the mean ± standard deviation.

Cumulative solute releases for subtidal mesocosms were calculated incrementally by multiplying the solute concentration at each sampling point by the total mesocosm liquid volume. For intertidal mesocosms which were periodically drained, cumulative releases were determined as solute concentration times liquid volume at each time of draining summed over all drainages. We assumed that solute concentrations reached equilibrium between sampling points and did not adjust values for potential dilution due to replenishing water volume removed through sampling in each mesocosm.

Results and discussion

Soil characteristics influenced by delta age and inundation patterns

Overall, transect position (supratidal *vs.* intertidal *vs.* subtidal) accounted for 51% of total variation in soil biogeochemical analytes ($F = 53, p < 0.001$), whereas transect location (OT *vs.* YT) accounted for 4% ($F = 8, p = 0.0097$). Within transects, soil C, N, and pH decreased in the order intertidal > supratidal > subtidal; the sole exception was soil pH in YT, where subtidal values were higher than in supratidal (Table 1). Total Fe oxides (SRO oxyhydroxides and LRO oxides) were high in the supratidal zones, particularly at the OT, and decreased with decreasing elevation. These values align with previously reported data from Mike Island (15–36 g kg^{-1} C; 1.2–2.6 g kg^{-1} N; 30–180 μmol g^{-1} Fe) and reflect higher overall concentrations of C, N, and Fe and lower pH in older delta regions.[17,49]

Short-range ordered and crystalline Fe oxides varied in abundance across both transects. Intertidal and subtidal soils contained primarily SRO Fe oxides, whereas supratidal soils had similar proportions of SRO and LRO Fe (~1 : 1 molar ratio). Higher relative proportions of SRO Fe oxides in intertidal and subtidal zones may (i) indicate rapid re-formation of metastable phases, offsetting transformation of SRO Fe to more crystalline LRO phases under successive redox cycles or (ii) retention of metastable phases under persistently anoxic subtidal conditions where transformation to crystalline oxides is kinetically limited.[28,50,51] This observation is consistent with previous findings that coastal wetlands are preferentially enriched in SRO Fe minerals relative to upland soils.[50] As deltaic islands gain elevation, soils transition from primarily anoxic conditions (subtidal) to variable anoxic–oxic cycles (intertidal) then primarily oxic conditions (supratidal),[11] thus, providing important evidence that differences in Fe abundance and mineral form across the transects illustrate that Fe redox cycling may play important and evolving roles in biogeochemical processes during delta formation.

CO_2 production enhanced by variable inundation

We investigated CO_2 production throughout the experiment to determine how inundation patterns affected organic matter

Table 1 Chemical properties of the bulk soil used for the incubation experiments. Concentrations of short-range ordered (SRO) and long-range ordered (LRO) Fe oxides were determined from selective chemical extractions. All values represent the mean ± standard deviation ($n = 3$). Letters represent significant differences within each column (Tukey HSD, $\alpha = 0.05$)

		Soil pH					SRO/LRO
Transect	Tidal zone	(−)	C (g kg^{-1})	N (g kg^{-1})	SRO Fe (μmol Fe g^{-1})	LRO Fe (μmol Fe g^{-1})[a]	(−)
Old	Supratidal	7.17 ± 0.01^{C}	37.6 ± 1.1^{B}	4.2 ± 0.3^{A}	139 ± 4^{C}	144 ± 8^{A}	1.0 ± 0.1
	Intertidal	7.18 ± 0.09^{BC}	48.6 ± 1.9^{A}	5.1 ± 0.1^{A}	101 ± 1^{A}	4 ± 5^{C}	3.0 ± 2.4
	Subtidal	7.16 ± 0.08^{C}	29.2 ± 1.1^{C}	1.7 ± 0.3^{B}	69 ± 1^{B}	13 ± 2^{C}	5.4 ± 1.1
Young	Supratidal	7.41 ± 0.13^{AC}	19.7 ± 0.7^{D}	1.3 ± 0.4^{B}	96 ± 1^{A}	85 ± 1^{B}	1.1 ± 0.1
	Intertidal	7.51 ± 0.15^{A}	20.4 ± 2.8^{D}	1.7 ± 0.2^{B}	85 ± 1^{D}	7 ± 1^{C}	4.7 ± 3.1
	Subtidal	7.49 ± 0.02^{AB}	18.1 ± 1.4^{D}	1.2 ± 0.3^{B}	59 ± 1^{E}	1 ± 2^{C}	5.4 ± 1.0

[a] Calculated as the difference between dithionite- and hydroxylamine-extractable Fe.

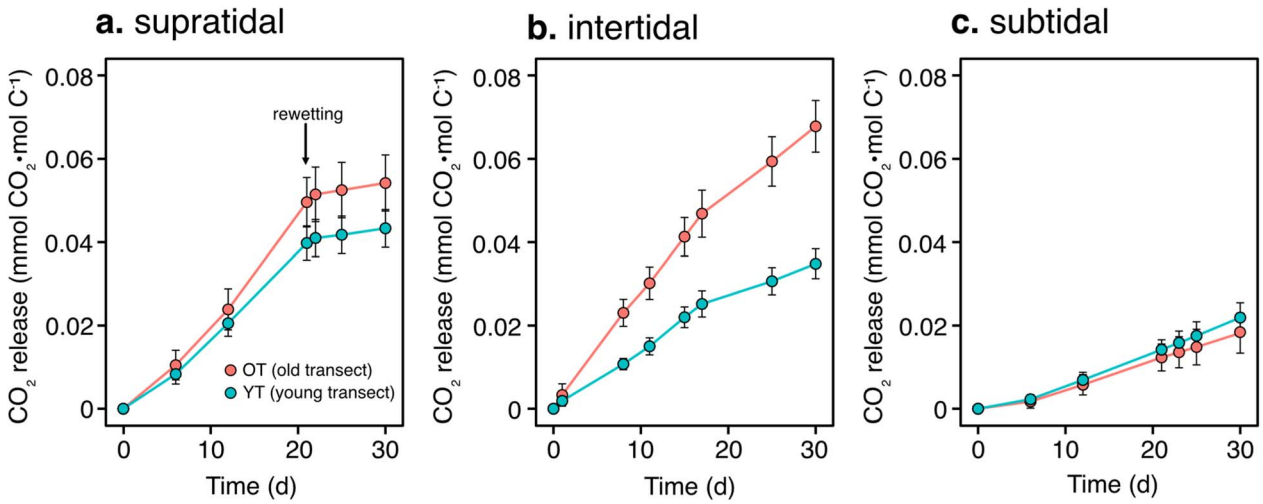

Fig. 3 Cumulative carbon dioxide (CO_2) release normalized to total soil C during (a) supratidal, (b) intertidal, and (c) subtidal incubations. Error bars represent standard deviation of the mean for triplicate mesocosms. The arrow in panel a indicates when supratidal soils were rewetted. The legend in panel a also applies to panels b–c.

decomposition, and whether these observations were consistent across space (OT *vs.* YT) and time (Fig. 3). Similar to soil properties, transect position accounted for significantly more of the total variation in both cumulative CO_2 release and average CO_2 flux ($F = 27.6$, $p < 0.001$) than transect location ($F = 4.8$, $p = 0.034$). In both OT and YT soils, supratidal and intertidal positions exhibited higher CO_2 production than subtidal soils (Fig. 4). Initial rates of CO_2 release were similar among OT and YT supratidal and OT intertidal soils and higher than YT intertidal soils. All observed trends in CO_2 flux were consistent whether fluxes were normalized on a molar (*i.e.*, mmol $CO_2 \cdot$mol C^{-1} d^{-1}), soil dry mass (mmol $CO_2 \cdot kg^{-1}$ d^{-1}), or surface area basis (mmol $CO_2 \cdot m^{-2}$ d^{-1}) (Table S1), indicating that differences in flux could be attributed to biogeochemical processes controlling organic matter decomposition rather than the quantity of organic matter.

Given the notable shift in CO_2 production after supratidal soils were rewetted (Fig. 3a), we analyzed all CO_2 fluxes separately for the time periods before (0–21 d) and after (22–30 d) supratidal rewetting to differentiate the relative effects of soil moisture and incubation time on CO_2 production (Fig. 4). Across both transects, average CO_2 fluxes from supratidal and intertidal soils were substantially lower during the second part of the incubation, with a decrease of approximately 85% in supratidal soils and 43% in intertidal soils. Meanwhile, subtidal CO_2 fluxes did not significantly change (Tukey HSD, $p > 0.05$). Although decreases in respiration in the supratidal zones may be an artifact of rewetting, decreasing CO_2 fluxes in intertidal

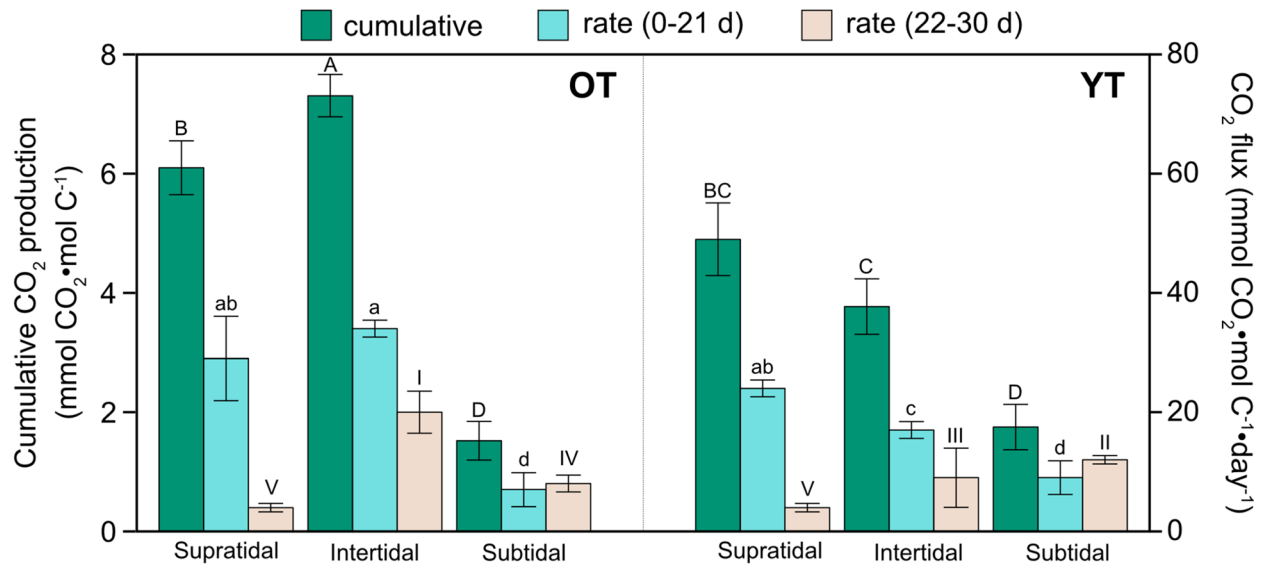

Fig. 4 CO_2 production across laboratory incubations. Cumulative CO_2 production is shown on the left vertical axis, and average fluxes are shown on the right vertical axis. Fluxes are grouped into days 0–21 and 22–30, corresponding to rewetting of supratidal soils. Bars labeled with different letters are statistically different (Tukey HSD, $\alpha = 0.05$).

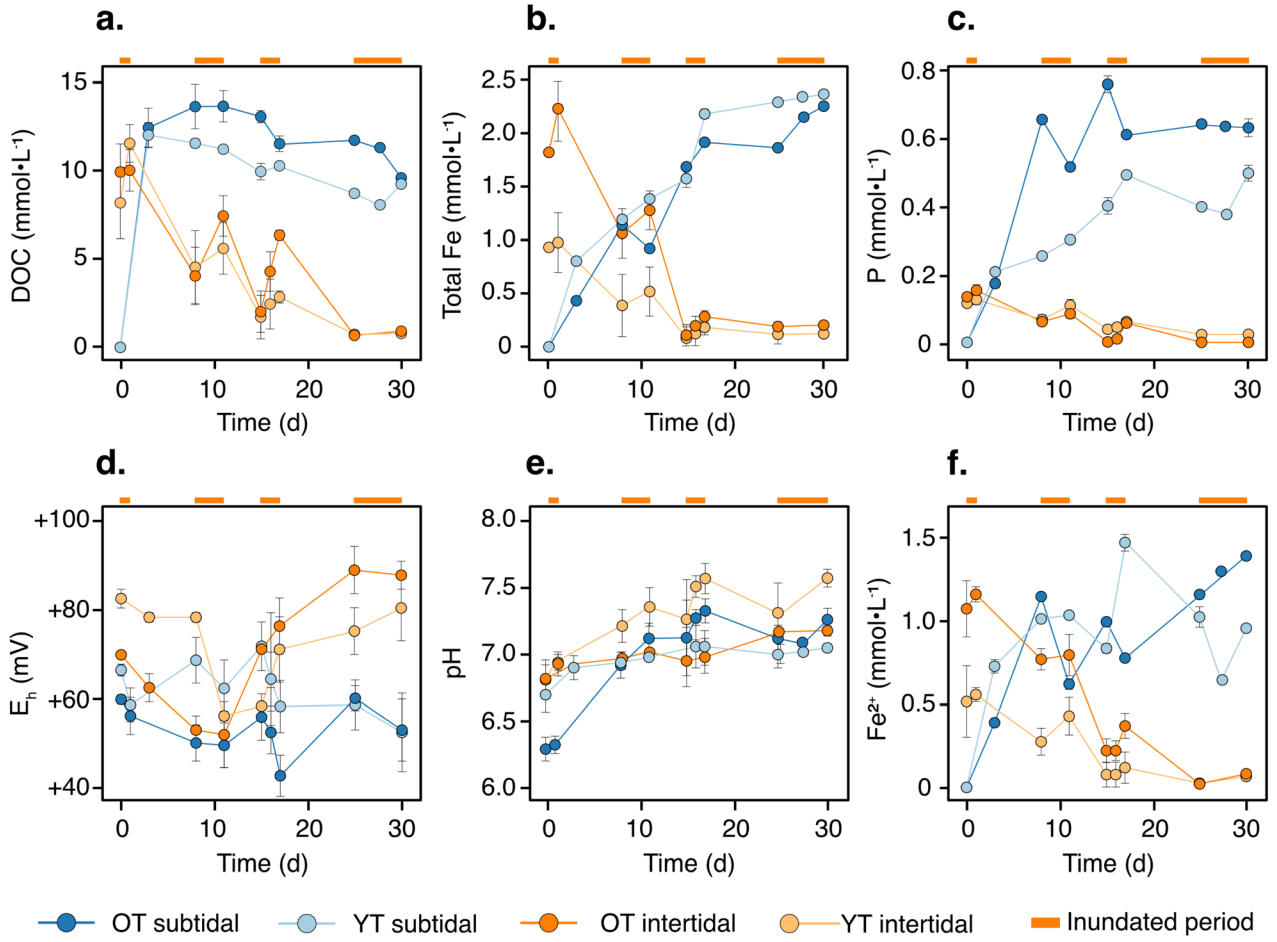

Fig. 5 Porewater measurements of (a) dissolved organic carbon (DOC; mmol L^{-1}), (b) total dissolved iron (Fe; mmol L^{-1}), and (c) dissolved phosphorus (P; mmol L^{-1}), (d) redox potential (E_h; mV *vs.* SHE), (e) pH, and (f) dissolved Fe^{2+} (mmol L^{-1}) during intertidal and subtidal incubations. Error bars represent standard deviations of triplicate mesocosms. The orange bars along the top axis represent inundated periods of intertidal incubations.

soils could result from decreases in carbon substrates over time. Microbial respiration in a closed system depletes bioavailable substrates, restricting further rates of organic matter decomposition.[52] However, the stable CO_2 fluxes for both subtidal incubations suggests that organic substrates did not become depleted under relatively low respiration rates. Persistent inundation may constrain rates of organic matter decomposition at the lowest elevation regardless of soil properties.

Solute mobilization across inundation gradients

Inundation patterns (*i.e.*, transect position) explained the majority of observed variability in porewater chemistry ($F = 6.5$, $p = 0.006$), with subtidal soils showing significantly lower cumulative releases of most solutes (DOC, Fe, P) than intertidal soils across both transects (Tukey HSD, $p > 0.05$). This pattern was consistent with CO_2 production ($F = 27.6$, $p < 0.001$; Fig. 4), indicating that prolonged inundation may reduce overall biogeochemical activity relative to drained or variably inundated conditions. In contrast, solute releases from intertidal soils varied with delta region, with higher releases of DOC, Fe, and P from intertidal soils for OT than YT, while Ca and Mg showed not significant differences between transects (Table S3).

Soil inundation was associated with distinct temporal patterns of solute concentrations that differed between intertidal and subtidal zones (Fig. 5). For subtidal soils, most analytes (Fe, P, Ca, pH) increased over time throughout the 30-day incubation, whereas DOC exhibited a sharp initial increase followed by a linear decrease (regression analysis; OT: $F = 21.98$, $p > 0.001$; YT: $F = 82.27$, $p > 0.001$) (Table S3). E_h remained relatively stable between +54 and +89 mV and cumulative solute releases were greater for OT than YT ($p > 0.05$). For intertidal soils, solute concentrations generally decreased over time but exhibited short pulses of solute release immediately following inundation. Porewater pH gradually increased while E_h values remained between +45 and +73 mV. Similar to subtidal soils, cumulative solute release from intertidal soils was higher for OT than YT ($p > 0.05$).

Cumulative releases of CO_2 and DOC, expressed as a fraction of total soil C, were compared in order to evaluate the potential for soils to lose C *via* CO_2 release or DOC leaching. Across all experiments, DOC loss outpaced CO_2 production by a factor of 10 to 67 (Table 2), reflecting the mobility of water-soluble

Table 2 Fractional loss of C during soil incubations. Values are shown as cumulative losses of C leached (DOC) or respired (CO_2) divided by the initial amount of C in the bulk soils. DOC : CO_2 are expressed on a molar basis. Values labeled with different letters are statistically different (Tukey HSD, $\alpha = 0.05$)

Transect	Position	DOC loss (%)	CO_2 loss (%)	DOC : CO_2
OT	Supratidal	—	0.02 ± 0.01^{B}	—
	Intertidal	2.30 ± 0.61^{A}	0.14 ± 0.02^{A}	16.4 ± 0.1^{B}
	Subtidal	0.94 ± 0.02^{B}	0.05 ± 0.04^{B}	18.8 ± 7.7^{B}
YT	Supratidal	—	0.01 ± 0.01^{B}	—
	Intertidal	2.52 ± 0.22^{A}	0.04 ± 0.02^{B}	63.0 ± 4.2^{A}
	Subtidal	1.08 ± 0.01^{B}	0.05 ± 0.03^{B}	21.6 ± 2.8^{B}

organic matter under inundated conditions. In contrast to individual patterns of CO_2 (Fig. 4) and DOC (Fig. 5a), transect location (OT *vs.* YT) had a stronger effect on DOC : CO_2 ratios ($F = 28.5$, $p = 0.004$) than transect position ($F = 4.4$, $p = 0.03$). Within transects, intertidal DOC : CO_2 values were higher than subtidal for YT (Tukey HSD, $p < 0.001$), while OT showed no significant difference between transect positions (Tukey HSD, $p = 0.618$). These differences in C loss pathways may reflect varying stages of ecosystem development and the balance between C accumulation and decomposition in emerging coastal deltas, as discussed below.

Processes regulating biogeochemical activity

The patterns of reduced biogeochemical activity in subtidal zones and enhanced activity in intertidal and supratidal zones are consistent with established conceptual models linking enhanced carbon cycling to environments that experience periodic redox fluctuations rather than persistently oxic or anoxic conditions.[53–57] In WLD, supratidal and intertidal soils are subject to redox shifts driven by episodic flooding and tidal exchange, respectively, whereas subtidal soils remain primarily inundated and anoxic.[58] Redox transitions in intermittently flooded soils can stimulate microbial metabolisms by increasing the availability of electron acceptors,[59,60] promoting organic matter turnover,[61–63] and regenerating reactive mineral phases,[64,65] thereby driving both CO_2 production and solute mobilization.[59] Thus, delta regions representing later stages of island development (*i.e.*, higher elevation relative to water level) are likely to support higher rates of biogeochemical activity than younger, predominantly subtidal areas. This linkage between elevation, inundation regime, and metabolic activity highlights

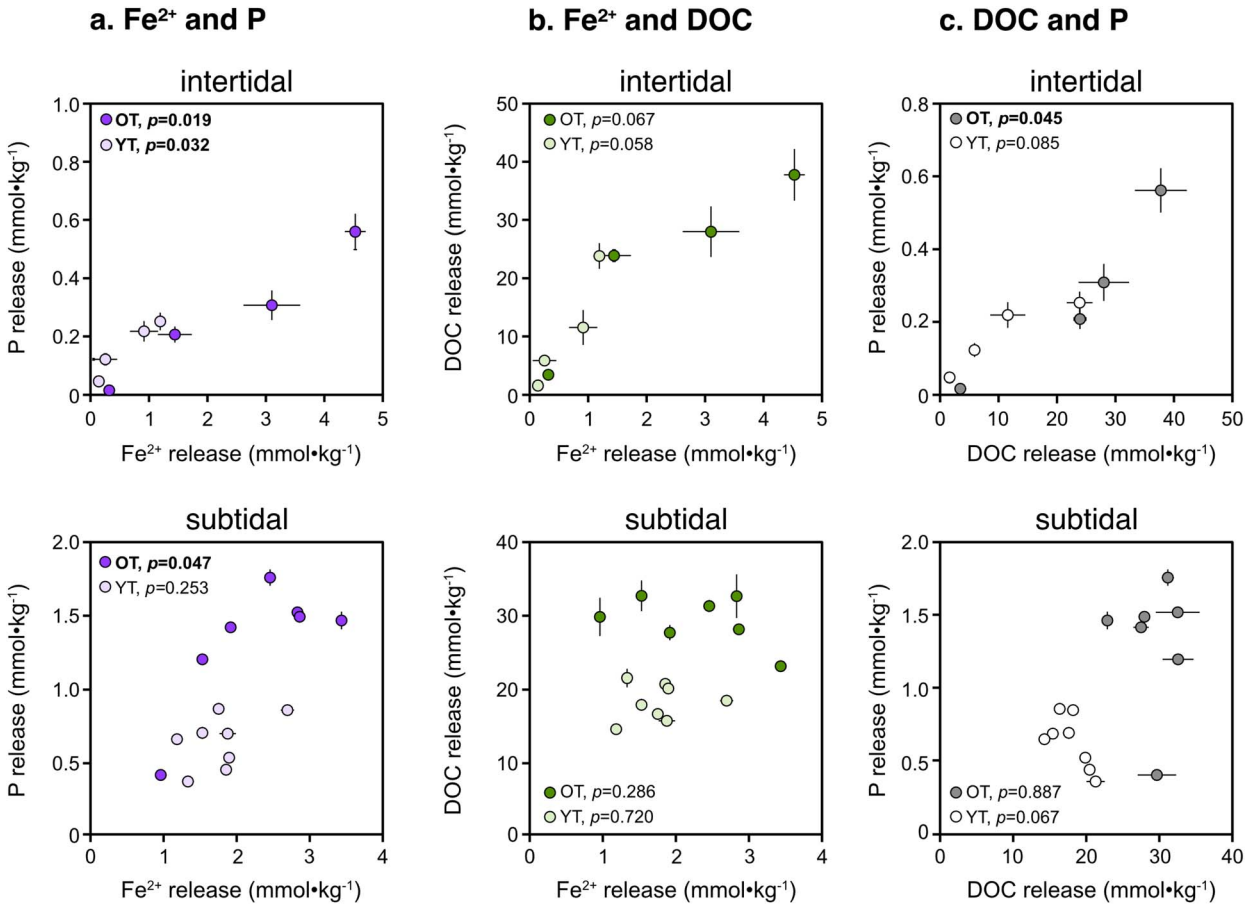

Fig. 6 Correlations between cumulative (a) Fe^{2+} and P, (b) Fe^{2+} and DOC, and (c) DOC and P release in intertidal and subtidal incubations. Error bars represent standard deviations of triplicate mesocosms. *P* values indicate goodness of fit for linear regression analysis ($\alpha = 0.05$). *P* values for significant linear correlations are shown in bold.

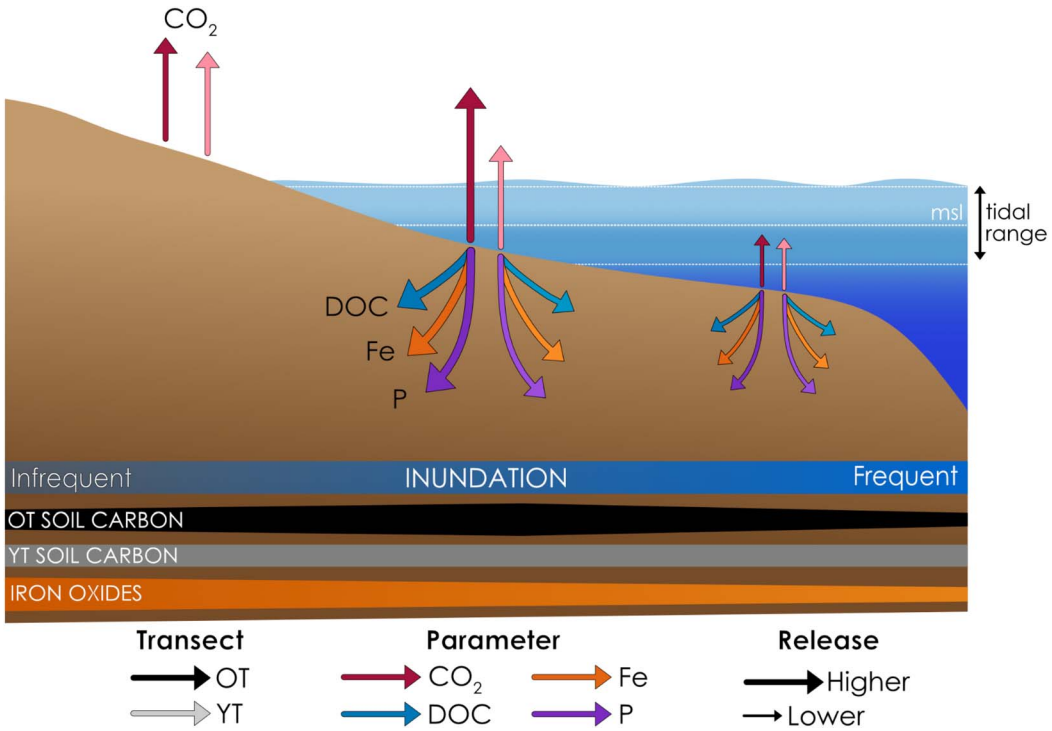

Fig. 7 Conceptual diagram of solute and carbon dioxide (CO_2) dynamics under variable inundation of freshwater coastal soils. The shaded blue area represents the tidal range, with more frequently inundated areas shown in darker colors. The white dashed lines represent mean sea level (msl), high tide, and low tide. Arrows represent the release of dissolved organic carbon (DOC), total dissolved iron (Fe) and phosphorus (P), and CO_2. Horizontal bars at the bottom of the figure indicate relative concentrations of total soil carbon and Fe(III) (oxyhydr)oxides. Note that porewater solutes could not be sampled in the supratidal soils.

the importance of geomorphic evolution in regulating carbon and nutrient cycling in active freshwater deltas.[10]

Successional development in WLD is further accompanied by systematic changes in soil chemistry and physical structure (Table 1).[10,66] Younger, frequently inundated soils are dominated by dense, mineral-rich riverine sediments, characterized by low organic C (1.7–2.4%) and N (0.08–0.18%) concentrations, and high C : N ratios. In contrast, as island elevation increases and inundation frequency decreases, soils transition toward more organic inputs from emergent vegetation, resulting in higher C (2.8–5.1%) and N (0.14–0.52%) concentrations with lower C : N ratios.[11,49,66] Reduced hydroperiods in supratidal and intertidal zones promote episodic oxygen exposure, enhance root penetration, and facilitate the development of more structurally complex and biogeochemically active soils.[67–69] These transitions in soil composition and structure likely amplify redox variability and substrate availability,[70] reinforcing higher rates of CO_2 production and solute mobilization in intertidal and supratidal soils. Collectively, our results indicate that inundation regime may exert an important control on carbon cycling during deltaic evolution.

Phosphorus retention modified by Fe redox cycling

The strong positive correlations between cumulative Fe^{2+} and P release (Fig. 6a and d; regression analysis, $p < 0.05$) suggest a strong influence of Fe oxides on P solubility, although organic matter or other minerals may also play an important role. Variable inundation across WLD drives frequent redox oscillations[58] that may promote the formation of SRO Fe oxides[71] with available surfaces for binding phosphate.[27,72] Further, persistent anoxia (*i.e.*, due to inundation) has been linked to microbial respiration of Fe oxides, potentially releasing large amounts of phosphate from WLD soils with comparatively low releases under aerobic (*e.g.*, drained) conditions.[15] The Fe reducing conditions (<100 mV at pH 7), increasing pH, and fluctuating Fe^{2+} concentrations in our study (Fig. 5d–f) were all key indicators of Fe redox cycling.[73,74] Thus, we infer that Fe reductive dissolution was an important source of P to the soil porewater in our study. Soil Fe oxides may also affect DOC mobility through sorption and co–precipitation interactions with organic matter;[17,75,76] however, Fe^{2+} and DOC correlations (Fig. 6c and d) were weaker than for Fe^{2+} and P, and linear (regression analysis, $p < 0.05$) only for intertidal soils, indicating that Fe reductive dissolution had a stronger influence on P retention than on DOC.

Organic matter decomposition may have also influenced P mobility in our experiments, with release of organic-P into porewater providing available substrates for phosphate cleavage by phosphatase enzymes.[77] Further, P may have interacted with species other than Fe oxides and organic matter entirely, including Ca, aluminum (Al), and non-oxide Fe. In coastal systems with high concentrations of Ca, Al, and dissolved Fe^{2+}, phosphate can sorb to Al- and Ca-oxides[72,78–80] or precipitate with metal cations to form compounds including

hydroxyapatite ($Ca_{10}(PO_4)_6(OH)_2$) and vivianite ($Fe^{II}_3(PO_4)_2 \cdot 8H_2O$).[81] Although these species can have a strong influence on P mobility in coastal wetlands, their capacity for P retention is determined primarily by changes in pH rather than fluctuations in E_h.[82–84] For example, the optimal pH range for P fixation is ~5–6 for Al and ~8–9 for Ca,[85] well outside the pH range in our study (6.4–7.7; Fig. 5e). In addition, our linear regression analyses revealed progressively weaker correlations of p(P, Fe) > p(P, DOC) > p(P, Ca), while Al concentrations were below the instrumental detection limit in all samples (data not shown). Overall, our results do not rule out the potential role of pH, base cations, and organic matter in regulating P mobility,[75,77,86] but support that Fe oxide cycling was the strongest contributor to P release of the measured analytes in our experiment.

Limitations to experimental approach

Due to logistical constraints, soil samples were frozen prior to analysis rather than analyzed fresh. Freezing can affect microbial activity[87] and Fe mineral characteristics;[88,89] however, all samples were treated identically and frozen for the same duration (~2 weeks), standardizing potential effects. Moreover, freezing has been shown to have minimal impact on overall soil biochemical properties.[87,90,91] We observed no significantly elevated CO_2 fluxes at early timepoints, indicating freezing artifacts did not prominently affect our results. Additionally, any changes to Fe oxide concentrations would have occurred uniformly across treatments, leaving our relative comparisons across inundation conditions unaffected.

We also emphasize that our P measurements by ICP-OES quantify total P and cannot differentiate between inorganic P (*i.e.*, phosphate) and P contained in organic matter (*i.e.*, organic P). This is an important distinction because inorganic phosphate is the readily bioavailable form or P while organic-P must be enzymatically cleaved from organic matter prior to microbial uptake.[92,93] As such, our data can reveal potential factors regulating P mobilization in emerging deltaic systems but cannot be used to directly infer bioavailability of the released P.

Conclusions

Emerging freshwater deltas experience dynamic hydrological regimes that may influence the fate of C and nutrients being exported from inland to open water systems. As deltas emerge, elevation gradients form that affect the frequency of soil inundation and could alter the interactions of OC and nutrients in the soil, and the biogeochemical processes that drive their transformation and/or release. This study improves our understanding of the potential influences of soil chemical properties and inundation on C and P release from emerging deltaic systems (Fig. 7). Our results suggest that older delta regions may supports higher rates of biogeochemical activity in supratidal and intertidal eco-hydrogeomorphic zones, presumably due to differences in soil chemical properties. Furthermore, inundation-driven redox oscillations in intertidal zones can enhance the decomposition of soil organic matter into carbon dioxide and accelerate the turnover of Fe(III) (oxyhydr) oxide minerals. In subtidal zones, soil saturation may restrict O_2 availability for OM decomposition and inhibit the formation of Fe–OC and Fe–P associations, exerting a stronger control over biogeochemical processes than soil properties. Microbial respiration of Fe oxides may be an important pathway for sustaining OM decomposition and P release under anoxic conditions. These results illustrate the interplay of hydrologic and geomorphic factors in delta soils, emphasizing the importance of emerging ecosystems as biogeochemical hotspots[94,95] – where redox shifts from water level fluctuations cause repeated Fe reductive dissolution under oxic conditions and precipitation of SRO Fe oxyhydroxides under oxic conditions,[71,96] As reactive Fe minerals can be a large part of total soil Fe in WLD and coastal ecosystems more broadly,[17,97] future work should address how Fe(III) phases will change over time, particular regarding their ability to influence carbon burial and buffer high nutrient loads from inland ecosystems.

Conflicts of interest

There are no conflicts to declare.

Data availability

A detailed description of the field site, additional experimental results, and all raw data supporting this article have been included as part of the supplementary information (SI). See DOI: https://doi.org/10.1039/d6em00129g.

Acknowledgements

We would like to thank Andre Rovai and Robert Twilley for access to field sites and assistance with site selection at Wax Lake Delta. In addition, we thank Michael Jones for assisting in the field collecting soil samples and student interns Kayla Summerlot and Georgie McDevitt for assisting with incubation experiments and soil processing. This work is supported by grant ERKPA45 through the U.S. Department of Energy, Office of Science, Office of Biological and Environmental Research, Environmental System Science program under Funding Opportunity DE-FOA-0002563. This manuscript has been authored by UT-Battelle, LLC, under contract DE-AC05-00OR22725 with the US Department of Energy (DOE). The US government retains and the publisher, by accepting the article for publication, acknowledges that the US government retains a nonexclusive, paid-up, irrevocable, worldwide license to publish or reproduce the published form of this manuscript, or allow others to do so, for US government purposes. DOE will provide public access to these results of federally sponsored research in accordance with the DOE Public Access Plan (https://www.energy.gov/doe-public-access-plan).

References

1 A. H. Sawyer, D. A. Edmonds and D. Knights, Surface Water-groundwater Connectivity in Deltaic Distributary Channel

Networks, *Geophys. Res. Lett.*, 2015, **42**, 10299–10306, DOI: 10.1002/2015gl066156.

2 A. M. Savoie, A. Moody, M. Gilbert, K. S. Dillon, S. D. Howden, A. M. Shiller and C. T. Hayes, Impact of Local Rivers on Coastal Acidification, *Limnol. Oceanogr.*, 2022, **67**(12), 2779–2795, DOI: 10.1002/lno.12237.

3 M. L. Kirwan and K. B. Gedan, Sea-Level Driven Land Conversion and the Formation of Ghost Forests, *Nat. Clim. Change*, 2019, **9**(6), 450–457, DOI: 10.1038/s41558-019-0488-7.

4 T. S. Bianchi, D. Butman, P. A. Raymond, N. D. Ward, R. J. S. Kates, K. W. Flessa, H. Zamora, A. R. Arellano, J. Ramirez and E. Rodriguez, The Experimental Flow to the Colorado River Delta: Effects on Carbon Mobilization in a Dry Watercourse, *J. Geophys. Res.:Biogeosci*, 2017, **122**(3), 607–627, DOI: 10.1002/2016JG003555.

5 B. D. Richter, J. V. Baumgartner, J. Powell and D. P. Braun, A Method for Assessing Hydrologic Alteration within Ecosystems, *Conserv. Biol.*, 1996, **10**(4), 1163–1174, DOI: 10.1046/j.1523-1739.1996.10041163.x.

6 J. W. Day, D. F. Boesch, E. J. Clairain, G. P. Kemp, S. B. Laska, W. J. Mitsch, K. Orth, H. Mashriqui, D. J. Reed, L. Shabman, C. A. Simenstad, B. J. Streever, R. R. Twilley, C. C. Watson, J. T. Wells and D. F. Whigham, Restoration of the Mississippi Delta: Lessons from Hurricanes Katrina and Rita, *Science*, 2007, **315**(5819), 1679–1684, DOI: 10.1126/science.1137030.

7 R. R. Twilley and V. Rivera-Monroy, Sediment and Nutrient Tradeoffs in Restoring Mississippi River Delta: Restoration vs Eutrophication, *J. Contemp. Water Res. Educ.*, 2009, **141**(1), 39–44, DOI: 10.1111/j.1936-704X.2009.00035.x.

8 E. Foufoula-Georgiou, J. Syvitski, C. Paola, C. T. Hoanh, P. Tuong, C. Vörösmarty, H. Kremer, E. Brondizio, Y. Saito and R. Twilley, International Year of Deltas 2013: A Proposal, *EOS Trans. Am. Geophys. Union*, 2011, **92**(40), 340–341, DOI: 10.1029/2011EO400006.

9 R. D. DeLaune, M. Kongchum, J. R. White and A. Jugsujinda, Freshwater Diversions as an Ecosystem Management Tool for Maintaining Soil Organic Matter Accretion in Coastal Marshes, *Catena*, 2013, **107**, 139–144, DOI: 10.1016/j.catena.2013.02.012.

10 R. R. Twilley, J. W. Day, A. E. Bevington, E. Castañeda-Moya, A. Christensen, G. Holm, L. R. Heffner, R. Lane, A. McCall, A. Aarons, S. Li, A. Freeman and A. S. Rovai, Ecogeomorphology of Coastal Deltaic Floodplains and Estuaries in an Active Delta: Insights from the Atchafalaya Coastal Basin, *Estuar. Coast Shelf Sci.*, 2019, **227**, 106341, DOI: 10.1016/j.ecss.2019.106341.

11 A. E. Bevington and R. R. Twilley, Island Edge Morphodynamics along a Chronosequence in a Prograding Deltaic Floodplain Wetland, *J. Coast Res.*, 2018, **34**(4), 806–817, DOI: 10.2112/JCOASTRES-D-17-00074.1.

12 W. Wagner, D. Lague, D. Mohrig, P. Passalacqua, J. Shaw and K. Moffett, Elevation Change and Stability on a Prograding Delta, *Geophys. Res. Lett.*, 2017, **44**(4), 1786–1794, DOI: 10.1002/2016GL072070.

13 D. Jensen, K. C. Cavanaugh, M. Simard, A. Christensen, A. Rovai and R. Twilley, Aboveground Biomass Distributions and Vegetation Composition Changes in Louisiana's Wax Lake Delta, *Estuar. Coast Shelf Sci.*, 2021, **250**, 107139, DOI: 10.1016/j.ecss.2020.107139.

14 M. V. Carle, L. Wang and C. E. Sasser, Mapping Freshwater Marsh Species Distributions Using WorldView-2 High-Resolution Multispectral Satellite Imagery, *Int. J. Rem. Sens.*, 2014, **35**(13), 4698–4716, DOI: 10.1080/01431161.2014.919685.

15 K. Upreti, K. Maiti and V. H. Rivera-Monroy, Microbial Mediated Sedimentary Phosphorus Mobilization in Emerging and Eroding Wetlands of Coastal Louisiana, *Sci. Total Environ.*, 2019, **651**(Pt 1), 122–133, DOI: 10.1016/j.scitotenv.2018.09.031.

16 K. Upreti, V. H. Rivera-Monroy, K. Maiti, A. E. Giblin and E. Castañeda-Moya, Dissimilatory Nitrate Reduction to Ammonium (DNRA) Is Marginal Relative to Denitrification in Emerging-Eroding Wetlands in a Subtropical Oligohaline and Eutrophic Coastal Delta, *Sci. Total Environ.*, 2022, **819**, 152942, DOI: 10.1016/j.scitotenv.2022.152942.

17 M. R. Shields, T. S. Bianchi, Y. Gélinas, M. A. Allison and R. R. Twilley, Enhanced Terrestrial Carbon Preservation Promoted by Reactive Iron in Deltaic Sediments, *Geophys. Res. Lett.*, 2016, **43**(3), 1149–1157, DOI: 10.1002/2015gl067388.

18 E. K. Coward, A. T. Thompson and A. F. Plante, Iron-Mediated Mineralogical Control of Organic Matter Accumulation in Tropical Soils, *Geoderma*, 2017, **306**, 206–216, DOI: 10.1016/j.geoderma.2017.07.026.

19 K. Lalonde, A. Mucci, A. Oullet and Y. Gélinas, Preservation of Organic Matter in Sediments Promoted by Iron, *Nature*, 2012, **483**, 198–200, DOI: 10.1038/nature10855.

20 K. R. Reddy; R. D. DeLaune and P. W. Inglett, *Biogeochemistry of Wetlands: Science and Applications*, CRC Press, Boca Raton, 2nd edn, 2022, DOI: 10.1201/9780429155833.

21 N. Sharma, Z. Wang, J. G. Catalano and D. E. Giammar, Dynamic Responses of Trace Metal Bioaccessibility to Fluctuating Redox Conditions in Wetland Soils and Stream Sediments, *ACS Earth Space Chem.*, 2022, **6**(5), 1331–1344, DOI: 10.1021/acsearthspacechem.2c00031.

22 M. Kleber, K. Eusterhues, M. Keiluweit, C. Mikutta, R. Mikutta and P. S. Nico, Mineral-Organic Associations: Formation, Properties, and Relevance in Soil Environments, *Adv. Agron.*, 2015, **130**, 1–420.

23 M. v. Lützow, I. Kögel-Knabner, K. Ekschmitt, E. Matzner, G. Guggenberger, B. Marschner and H. Flessa, Stabilization of Organic Matter in Temperate Soils: Mechanisms and Their Relevance under Different Soil Conditions – a Review, *Eur. J. Soil Sci.*, 2006, **57**(4), 426–445, DOI: 10.1111/j.1365-2389.2006.00809.x.

24 E. K. Coward, T. Ohno and A. F. Plante, Adsorption and Molecular Fractionation of Dissolved Organic Matter on Iron-Bearing Mineral Matrices of Varying Crystallinity, *Environ. Sci. Technol.*, 2018, **52**(3), 1036–1044, DOI: 10.1021/acs.est.7b04953.

25 E. K. Coward, T. Ohno and D. L. Sparks, Direct Evidence for Temporal Molecular Fractionation of Dissolved Organic Matter at the Iron Oxyhydroxide Interface, *Environ. Sci. Technol.*, 2019, **53**(2), 642–650, DOI: 10.1021/acs.est.8b04687.

26 E. Herndon, A. AlBashaireh, D. Singer, T. Roy Chowdhury, B. Gu and D. Graham, Influence of Iron Redox Cycling on Organo-Mineral Associations in Arctic Tundra Soil, *Geochim. Cosmochim. Acta*, 2017, **207**, 210–231, DOI: 10.1016/j.gca.2017.02.034.

27 E. M. Herndon, L. Kinsman-Costello, K. A. Duroe, J. Mills, E. S. Kane, S. D. Sebestyen, A. A. Thompson and S. D. Wullschleger, Iron (Oxyhydr)Oxides Serve as Phosphate Traps in Tundra and Boreal Peat Soils, *J. Geophys. Res.:Biogeosci*, 2019, **124**(2), 227–246, DOI: 10.1029/2018jg004776.

28 A. Bhattacharyya, A. N. Campbell, M. M. Tfaily, Y. Lin, R. K. Kukkadapu, W. L. Silver, P. S. Nico and J. Pett-Ridge, Redox Fluctuations Control the Coupled Cycling of Iron and Carbon in Tropical Forest Soils, *Environ. Sci. Technol.*, 2018, **52**(24), 14129–14139, DOI: 10.1021/acs.est.8b03408.

29 NOAA National Climatic Data Center, *Global Summary of the Year*, Morgan City, LA, 2024, https://www.ncei.noaa.gov/cdo-web/datasets/GSOY/stations/GHCND:USC00166394/detail.

30 R. A. Davidson, *Wax Lake Outlet Control Structure Louisiana: Hydraulic Model Investigation; Technical Report HL-88-23*, US Army Corps of Engineers: Vicksburg, MS, 1988.

31 W. Kim, D. Mohrig, R. Twilley, C. Paola and G. Parker, Is It Feasible to Build New Land in the Mississippi River Delta?, *EOS Trans. Am. Geophys. Union*, 2009, **90**(42), 373–374, DOI: 10.1029/2009EO420001.

32 C. G. Fichot; J. Harringmeyer; M. Weiser Delta-X: In Situ Water Quality Indicators across MRD, LA, USA, 2021, Version 2, 2022, DOI: 10.3334/ORNLDAAC/2080.

33 H. H. Roberts and J. Sneider, *Atchafalaya-Wax Lake Deltas : The New Regressive Phase of the Mississippi River Delta Complex*, Louisiana Geological Survey, 2003, Guidebook series no. 6.

34 Y. C. Allen, B. R. Couvillion and J. A. Barras, Using Multitemporal Remote Sensing Imagery and Inundation Measures to Improve Land Change Estimates in Coastal Wetlands, *Estuaries Coasts*, 2012, **35**(1), 190–200, DOI: 10.1007/s12237-011-9437-z.

35 R. Twilley, A. Fontenot-Cassaway, A. Rovai, *Delta-X: Feldspar Sediment Accretion Measurements, MRD, LA, USA, 2019–2023, Version 3.*, ORNL DAAC, Oak Ridge, Tennessee, USA, DOI: 10.3334/ORNLDAAC/2290.

36 M. R. Shields, T. S. Bianchi, D. Mohrig, J. A. Hutchings, W. F. Kenney, A. S. Kolker and J. H. Curtis, Carbon Storage in the Mississippi River Delta Enhanced by Environmental Engineering, *Nat. Geosci.*, 2017, **10**, 846–851, DOI: 10.1038/ngeo3044.

37 J. B. Shaw, D. Mohrig and S. K. Whitman, The Morphology and Evolution of Channels on the Wax Lake Delta, Louisiana, USA, *J. Geophys. Res. Earth Surf.*, 2013, **118**(3), 1562–1584, DOI: 10.1002/jgrf.20123.

38 J. B. Shaw and D. Mohrig, The Importance of Erosion in Distributary Channel Network Growth, Wax Lake Delta, Louisiana, USA, *Geology*, 2014, **42**(1), 31–34, DOI: 10.1130/G34751.1.

39 G. O. Holm and C. E. Sasser, Differential Salinity Response between Two Mississippi River Subdeltas: Implications for Changes in Plant Composition, *Estuaries*, 2001, **24**(1), 78–89, DOI: 10.2307/1352815.

40 G. P. Shaffer, C. E. Sasser, J. G. Gosselink and M. Rejmanek, Vegetation Dynamics in the Emerging Atchafalaya Delta, Louisiana, USA, *J. Ecol.*, 1992, **80**(4), 677–687, DOI: 10.2307/2260859.

41 H. Ma, L. G. Larsen and R. W. Wagner, Ecogeomorphic Feedbacks That Grow Deltas, *J. Geophys. Res. Earth Surf.*, 2018, **123**(12), 3228–3250, DOI: 10.1029/2018JF004706.

42 E. A. Olliver and D. A. Edmunds, Defining the Ecogeomorphic Succession of Land Building for Freshwater, Intertidal Wetlands in Wax Lake Delta, Louisiana, *Estuar. Coast Shelf Sci.*, 2017, **196**, 45–57, DOI: 10.1016/j.ecss.2017.06.009.

43 M. Carle, Spatial Structure and Dynamics of the Plant Communities in a Pro-grading River Delta: Wax Lake Delta. Atchafalaya Bay, LA, Doctoral thesis, Louisiana State University, 2013.

44 S. W. Poulton and D. E. Canfield, Development of a Sequential Extraction Procedure for Iron: Implications for Iron Partitioning in Continentally Derived Particulates, *Chem. Geol.*, 2005, **214**(3), 209–221, DOI: 10.1016/j.chemgeo.2004.09.003.

45 E. Herndon, L. Kinsman-Costello, N. Di Domenico, K. Duroe, M. Barczok, C. Smith and S. D. Wullschleger, Iron and Iron-Bound Phosphate Accumulate in Surface Soils of Ice-Wedge Polygons in Arctic Tundra, *Environ. Sci. Process. Impacts*, 2020, **22**(7), 1475–1490, DOI: 10.1039/d0em00142b.

46 American Public Health Association, American Water Works Association, Water Environment Federation, *Standard Methods for the Examination of Water and Wastewater*, ed. W. C. Lipps, E. B. Braun-Howland and T. E. Baxter, APHA Press, Washington DC, 24th edn, 2023.

47 *R Core Team. R: A Language and Environment for Statistical Computing*, 2023. https://www.R-project.org/.

48 H. Wickham *Ggplot2: Elegant Graphics for Data Analysis*, Springer-Verlag, New York, 2016.

49 E. Castañeda-Moya and E. Solohin, *Delta-X: Soil Properties for Herbaceous Wetlands, MRD, Louisiana, 2021, V3*, ORNL DAAC, Oak Ridge, Tennessee, USA, 2023, DOI: 10.3334/ORNLDAAC/2239.

50 H. Ma, A. Thompson, S. J. Hall, J. Wang, Y. Xiao, C.-Q. Liu and C. Chen, Enrichment of Metastable Iron Minerals in Global Coastal Wetlands, *Nat. Geosci.*, 2025, **18**, 885–892, DOI: 10.1038/s41561-025-01764-7.

51 A. Thompson, O. A. Chadwick, D. G. Rancourt and J. Chorover, Iron-Oxide Crystallinity Increases during Soil Redox Oscillations, *Geochim. Cosmochim. Acta*, 2006, **70**(7), 1710–1727, DOI: 10.1016/j.gca.2005.12.005.

52 Y. Lin, A. N. Campbell, A. Bhattacharyya, N. DiDonato, A. M. Thompson, M. M. Tfaily, P. S. Nico, W. L. Silver and J. Pett-Ridge, Differential Effects of Redox Conditions on the Decomposition of Litter and Soil Organic Matter, *Biogeochemistry*, 2021, **154**(1), 1–15, DOI: 10.1007/s10533-021-00790-y.

53 K. R. Reddy and W. H. Patrick, Effect of Alternate Aerobic and Anaerobic Conditions on Redox Potential, Organic Matter Decomposition and Nitrogen Loss in a Flooded Soil, *Soil Biol. Biochem.*, 1975, **7**(2), 87–94, DOI: 10.1016/0038-0717(75)90004-8.

54 J. H. Crane and F. S. Davies, Periodic and Seasonal Flooding Effects on Survival, Growth, and Stomatal Conductance of Young Rabbiteye Blueberry Plants, *J. Am. Soc. Hortic. Sci.*, 1988, **113**(4), 488–493, DOI: 10.21273/JASHS.113.4.488.

55 K. A. Ballantine, P. M. Groffman, J. Lehmann and R. L. Schneider, Stimulating Nitrate Removal Processes of Restored Wetlands, *Environ. Sci. Technol.*, 2014, **48**(13), 7365–7373, DOI: 10.1021/es500799v.

56 M. L. Kirwan, J. A. Langley, G. R. Guntenspergen and J. P. Megonigal, The Impact of Sea-Level Rise on Organic Matter Decay Rates in Chesapeake Bay Brackish Tidal Marshes, *Biogeosciences*, 2013, **10**(3), 1869–1876, DOI: 10.5194/bg-10-1869-2013.

57 C. L. Stagg, D. R. Schoolmaster, K. W. Krauss, N. Cormier and W. H. Conner, Causal Mechanisms of Soil Organic Matter Decomposition: Deconstructing Salinity and Flooding Impacts in Coastal Wetlands, *Ecology*, 2017, **98**(8), 2003–2018, DOI: 10.1002/ecy.1890.

58 E. Herndon, M. J. Berens, R. M. Pilla and G. Schwaner, Temporal Patterns in Soil Redox Potential Vary Across a Freshwater Coastal Delta, *Hydrol. Process.*, 2025, **39**(11), e70338, DOI: 10.1002/hyp.70338.

59 A. Thompson, O. A. Chadwick, S. Boman and J. Chorover, Colloid Mobilization During Soil Iron Redox Oscillations, *Environ. Sci. Technol.*, 2006, **40**(18), 5743–5749, DOI: 10.1021/es061203b.

60 S. K. Chapman, M. A. Hayes, B. Kelly and J. A. Langley, Exploring the Oxygen Sensitivity of Wetland Soil Carbon Mineralization, *Biol. Lett.*, 2019, **15**, 20180407, DOI: 10.1098/rsbl.2018.0407.

61 K. Boye, A. M. Herrmann, M. V. Schaefer, M. M. Tfaily and S. Fendorf, Discerning Microbially Mediated Processes During Redox Transitions in Flooded Soils Using Carbon and Energy Balances, *Front. Environ. Sci.*, 2018, **6**, 15, DOI: 10.3389/fenvs.2018.00015.

62 S. M. Dunham-Cheatham, Q. Zhao, D. Obrist and Y. Yang, Unexpected Mechanism for Glucose-Primed Soil Organic Carbon Mineralization under an Anaerobic–Aerobic Transition, *Geoderma*, 2020, **376**, 114535, DOI: 10.1016/j.geoderma.2020.114535.

63 C. Chen, S. J. Hall, E. Coward and A. Thompson, Iron-Mediated Organic Matter Decomposition in Humid Soils Can Counteract Protection, *Nat. Commun.*, 2020, **11**(1), 2255, DOI: 10.1038/s41467-020-16071-5.

64 Z. Xu and D. C. W. Tsang, Mineral-Mediated Stability of Organic Carbon in Soil and Relevant Interaction Mechanisms, *Eco-Environ. Health*, 2024, **3**(1), 59–76, DOI: 10.1016/j.eehl.2023.12.003.

65 M. S. Patzner, C. W. Mueller, M. Malusova, M. Baur, V. Nikeleit, T. Scholten, C. Hoeschen, J. M. Byrne, T. Borch, A. Kappler and C. Bryce, Iron Mineral Dissolution Releases Iron and Associated Organic Carbon during Permafrost Thaw, *Nat. Commun.*, 2020, **11**(1), 6329, DOI: 10.1038/s41467-020-20102-6.

66 M. R. Shields, T. S. Bianchi, A. S. Kolker, W. F. Kenney, D. Mohrig, T. Z. Osborne and J. H. Curtis, Factors Controlling Storage, Sources, and Diagenetic State of Organic Carbon in a Prograding Subaerial Delta: Wax Lake Delta, Louisiana, *J. Geophys. Res.:Biogeosci*, 2019, **124**(5), 1115–1131, DOI: 10.1029/2018JG004683.

67 K. W. Krauss, T. W. Doyle, R. R. Twilley, V. H. Rivera-Monroy and J. K. Sullivan, Evaluating the Relative Contributions of Hydroperiod and Soil Fertility on Growth of South Florida Mangroves, *Hydrobiologia*, 2006, **569**(1), 311–324, DOI: 10.1007/s10750-006-0139-7.

68 B. M. Conroy, J. J. Kelleway and K. Rogers, Root Productivity Contributes to Carbon Storage and Surface Elevation Adjustments in Coastal Wetlands, *Plant Soil*, 2025, **513**(1), 605–631, DOI: 10.1007/s11104-025-07204-0.

69 E. Kristensen; R. M. Connolly; X. L. Otero; C. Marchand; T. O. Ferreira; V. H. Rivera-Monroy Biogeochemical Cycles: Global Approaches and Perspectives. in *Mangrove Ecosystems: A Global Biogeographic Perspective*, ed.V. H. Rivera-Monroy, S. Y. Lee, E. Kristensen, R. R. Twilley, Springer International Publishing, Cham, 2017, pp 163–209. doi: DOI: 10.1007/978-3-319-62206-4_6.

70 S. Cui, P. Liu, H. Guo, C. K. Nielsen, J. W. M. Pullens, Q. Chen, L. Pugliese and S. Wu, Wetland Hydrological Dynamics and Methane Emissions, *Commun. Earth Environ.*, 2024, **5**(1), 470, DOI: 10.1038/s43247-024-01635-w.

71 S. Ellery, W. Ellery, H. Tsikos and J. Dunlevey, Depression Wetland Formation by Redox-Driven Iron and Silica Cycling, *Wetl. Ecol. Manag.*, 2024, **32**(2), 191–206, DOI: 10.1007/s11273-023-09968-7.

72 A. K. Darke and M. R. Walbridge, Al and Fe Biogeochemistry in a Floodplain Forest: Implications for P Retention, *Biogeochemistry*, 2000, **51**, 1–32, DOI: 10.1023/A:1006302600347.

73 W. L. Lindsay Solubility and Redox Equilibria of Iron Compounds in Soils. in *Iron in Soils and Clay Minerals*, ed J. W. Stucki, B. A. Goodman, U. Schwertmann, Springer Netherlands, Dordrecht, 1988, pp 37–62, DOI: 10.1007/978-94-009-4007-9_3.

74 D. R. Lovley and E. J. P. Phillips, Novel Mode of Microbial Energy Metabolism: Organic Carbon Oxidation Coupled to Dissimilatory Reduction of Iron or Manganese, *Appl. Environ. Microbiol.*, 1988, **54**(6), 1472–1480, DOI: 10.1128/aem.54.6.1472-1480.1988.

75 K. J. Gibbons and T. B. Bridgeman, Effect of Temperature on Phosphorus Flux from Anoxic Western Lake Erie Sediments, *Water Res.*, 2020, **182**, 116022, DOI: 10.1016/j.watres.2020.116022.

76 *Iron in Soils and Clay Minerals*, ed J. W. Stucki, B. A. Goodman, U. Schwertmann, Springer Netherlands, Dordrecht, 1st edn, 1987, DOI: 10.1007/978-94-009-4007-9.
77 R. N. Sah and D. S. Mikkelsen, Phosphorus Behavior in Flooded-Drained Soils. I. Effects on Phosphorus Sorption, *Soil Sci. Soc. Am. J.*, 1989, **53**(6), 1718–1722, DOI: 10.2136/sssaj1989.03615995005300060018x.
78 C. Paludan and J. T. Morris, Distribution and Speciation of Phosphorus along a Salinity Gradient in Intertidal Marsh Sediments, *Biogeochemistry*, 1999, **45**(2), 197–221, DOI: 10.1007/BF01106781.
79 O. A. Diaz, K. R. Reddy and P. A. Moore, Solubility of Inorganic Phosphorus in Stream Water as Influenced by pH and Calcium Concentration, *Water Res.*, 1994, **28**(8), 1755–1763, DOI: 10.1016/0043-1354(94)90248-8.
80 P. V. Sundareshwar and J. T. Morris, Phosphorus Sorption Characteristics of Intertidal Marsh Sediments along an Estuarine Salinity Gradient, *Limnol. Oceanogr.*, 1999, **44**(7), 1693–1701, DOI: 10.4319/lo.1999.44.7.1693.
81 D. W. O'Connell, M. Mark Jensen, R. Jakobsen, B. Thamdrup, T. Joest Andersen, A. Kovacs and H. C. Bruun Hansen, Vivianite Formation and Its Role in Phosphorus Retention in Lake Ørn, Denmark, *Chem. Geol.*, 2015, **409**, 42–53, DOI: 10.1016/j.chemgeo.2015.05.002.
82 M. Aeppli, S. Vranic, R. Kaegi, R. Kretzschmar, A. R. Brown, A. Voegelin, T. B. Hofstetter and M. Sander, Decreases in Iron Oxide Reducibility during Microbial Reductive Dissolution and Transformation of Ferrihydrite, *Environ. Sci. Technol.*, 2019, **53**(15), 8736–8746, DOI: 10.1021/acs.est.9b01299.
83 M. Aeschbacher, C. Graf, R. P. Schwarzenbach and M. Sander, Antioxidant Properties of Humic Substances, *Environ. Sci. Technol.*, 2012, **46**(9), 4916–4925, DOI: 10.1021/es300039h.
84 D. R. Lovley, J. D. Coates, E. L. Blunt-Harris, E. J. P. Phillips and J. C. Woodward, Humic Substances as Electron Acceptors for Microbial Respiration, *Nature*, 1996, **382**(6590), 445–448, DOI: 10.1038/382445a0.
85 C. Penn and J. Camberato, A Critical Review on Soil Chemical Processes That Control How Soil pH Affects Phosphorus Availability to Plants, *Agriculture*, 2019, **9**(6), 120, DOI: 10.3390/agriculture9060120.
86 I. C. R. Holford and W. H. Patrick, Effects of Reduction and pH Changes on Phosphate Sorption and Mobility in an Acid Soil, *Soil Sci. Soc. Am. J.*, 1979, **43**(2), 292–297, DOI: 10.2136/sssaj1979.03615995004300020010x.
87 B. Stenberg, M. Johansson, M. Pell, K. Sjödahl-Svensson, J. Stenström and L. Torstensson, Microbial Biomass and Activities in Soil as Affected by Frozen and Cold Storage, *Soil Biol. Biochem.*, 1998, **30**(3), 393–402, DOI: 10.1016/S0038-0717(97)00125-9.
88 A. P. Sebaaly, F. Van Rijn, K. Hanna and J.-F. Boily, Ice as a Kinetic and Mechanistic Driver of Oxalate-Promoted Iron Oxyhydroxide Dissolution, *Proc. Natl. Acad. Sci. U. S. A.*, 2025, **122**(35), e2507588122, DOI: 10.1073/pnas.2507588122.
89 D. Jeong, K. Kim and W. Choi, Accelerated Dissolution of Iron Oxides in Ice, *Atmos. Chem. Phys.*, 2012, **12**(22), 11125–11133, DOI: 10.5194/acp-12-11125-2012.
90 M. Goberna, H. Insam, J. A. Pascual and J. Sánchez, Storage Effects on the Community Level Physiological Profiles of Mediterranean Forest Soils, *Soil Biol. Biochem.*, 2005, **37**(1), 173–178, DOI: 10.1016/j.soilbio.2004.06.014.
91 M. S. Peoples and R. T. Koide, Considerations in the Storage of Soil Samples for Enzyme Activity Analysis, *Appl. Soil Ecol.*, 2012, **62**, 98–102, DOI: 10.1016/j.apsoil.2012.08.002.
92 M. Hu, R. Yan, H. Wu, R. Ni, D. Zhang and S. Zou, Linking Soil Phosphorus Availability and Phosphatase Functional Genes to Coastal Marsh Erosion: Implications for Nutrient Cycling and Wetland Restoration, *Sci. Total Environ.*, 2023, **898**, 165559, DOI: 10.1016/j.scitotenv.2023.165559.
93 P. Nannipieri; L. Giagnoni; L. Landi; G. Renella Role of Phosphatase Enzymes in Soil. In *Phosphorus in Action: Biological Processes in Soil Phosphorus Cycling*, ed E. Bünemann, A. Oberson, E. Frossard, Soil Biology; Springer, Berlin, Heidelberg, 2011; pp pp 215–243, DOI: 10.1007/978-3-642-15271-9_9.
94 E. S. Bernhardt, J. R. Blaszczak, C. D. Ficken, M. L. Fork, K. E. Kaiser and E. C. Seybold, Control Points in Ecosystems: Moving Beyond the Hot Spot Hot Moment Concept, *Ecosystems*, 2017, **20**(4), 665–682, DOI: 10.1007/s10021-016-0103-y.
95 K. F. Patel, A. Malhotra, C. G. Norris, S. A. McKever, D. M. Fields, J. I. Musci, S. Bandopadhyay, B. Bond-Lamberty, X. Chen, D. J. Day, K. O. Doro, E. Fluet-Chouinard, M. Garcia, K. M. Kemner, F. Machado-Silva, N. McDowell, K. A. Morris, A. Myers-Pigg, E. J. O'Loughlin, T. O'Meara, R. B. Peixoto, S. C. Pennington, P. Regier, R. Rich, K. A. Rod, B. Sulman, P. Thornton, N. Ward, S. J. Wilson, M. N. Weintraub, J. P. Megonigal and V. L. Bailey, Transition Zones at the Changing Coastal Terrestrial-Aquatic Interface, *J. Geophys. Res.:Biogeosci*, 2025, **130**(11), e2025JG008978, DOI: 10.1029/2025JG008978.
96 A. Thompson, D. G. Rancourt, O. A. Chadwick and J. Chorover, Iron Solid-Phase Differentiation along a Redox Gradient in Basaltic Soils, *Geochim. Cosmochim. Acta*, 2011, **75**(1), 119–133, DOI: 10.1016/j.gca.2010.10.005.
97 C. Yu, S. Xie, Z. Song, S. Xia and M. E. Åström, Biogeochemical Cycling of Iron (Hydr-)Oxides and Its Impact on Organic Carbon Turnover in Coastal Wetlands: A Global Synthesis and Perspective, *Earth-Sci. Rev.*, 2021, **218**, 103658, DOI: 10.1016/j.earscirev.2021.103658.